

## Propagation of a Glow Discharge into the Annular Gap between the Discharge Tube Wall and the Cathode

Harry Veron and Nathan Wainfan

Citation: *Journal of Applied Physics* **37**, 836 (1966); doi: 10.1063/1.1708268

View online: <http://dx.doi.org/10.1063/1.1708268>

View Table of Contents: <http://scitation.aip.org/content/aip/journal/jap/37/2?ver=pdfcov>

Published by the **AIP Publishing**

---

### Articles you may be interested in

[Power balance at cathode in glow discharges](#)

*Phys. Plasmas* **12**, 113502 (2005); 10.1063/1.2127929

[New Hollow Cathode Glow Discharge](#)

*J. Appl. Phys.* **30**, 711 (1959); 10.1063/1.1735220

[The Role of Cathode Temperature in the Glow Discharge](#)

*J. Appl. Phys.* **21**, 681 (1950); 10.1063/1.1699731


[Dynamic Characteristics of Glow Discharge Tubes](#)

*J. Appl. Phys.* **9**, 421 (1938); 10.1063/1.1710435

[The Cathode Region in the Glow Discharge](#)

*J. Appl. Phys.* **8**, 779 (1937); 10.1063/1.1710254

---

The Shimadzu logo, consisting of a stylized 'S' inside a circle.**SHIMADZU**  
Excellence in Science

**Powerful, Multi-functional UV-Vis-NIR and FTIR Spectrophotometers**

Providing the utmost in sensitivity, accuracy and resolution for applications in materials characterization and nano research

- Photovoltaics
- Polymers
- Thin films
- Paints
- Ceramics
- DNA film structures
- Coatings
- Packaging materials

[Click here to learn more](#)

A row of four Shimadzu spectrophotometers. From left to right: a small benchtop model, a larger benchtop model with a sample holder, a large floor-standing model with a sample holder, and a large floor-standing model with a sample holder.

## DISCUSSION AND SUMMARY

Crystals of ruby which are strain free and very low in dislocation density can be grown from molten lead fluoride solutions. Although these crystals are of high optical quality, they do contain a concentration gradient in chromium. One of the sources of this gradient is the tendency of  $\text{Cr}^{3+}$  to form  $\text{Cr}^{6+}$  as the temperature of the  $\text{PbF}_2$  solution is lowered.  $\text{Cr}^{6+}$  does not substitute for  $\text{Al}^{3+}$  in  $\text{Al}_2\text{O}_3$ .

Ruby crystal growth from flux tends to be extremely anisotropic with little or no growth along the  $C$  axis. It was found that while the plates grown under large temperature gradients had a significantly greater  $C$ -axis growth, there is still an undesirably large level of flux inclusions. It is felt that these inclusions result from minor, localized temperature fluctuations which are difficult to eliminate. There is some indication also that the addition of 3 wt %  $\text{B}_2\text{O}_3$  to the  $\text{PbF}_2$  reduces the tendency to incorporate flux in the crystals.<sup>8</sup>

<sup>8</sup> L. G. Van Uitert, W. H. Grodkiewicz, and E. F. Dearborn, *Extended Abstracts, Electronics Division of the Electrochemical Society*, Vol. 13, No. 1 (1964).

The occurrence of line broadening in undoped-fluoride-substituted ruby was an unexpected dividend. It does, however, present the necessity of growing narrow linewidth ruby from  $\text{PbO}$ -rich fluxes. It was noted that an optimum lies between 0.5 and 2.0 mole %  $\text{Ga}_2\text{O}_3$ . Concentrations below this level have little or no effect on the linewidth while higher concentrations of Ga apparently no longer create a statistical distribution of fields around the  $\text{Cr}^{3+}$  ions; instead, discrete entities are set up which partly return the spectrum to the sharp line type, only much more complicated.

## ACKNOWLEDGMENTS

This work was supported by the U. S. Office of Naval Research. We wish to thank W. Spencer and R. L. Barns of the Bell Telephone Laboratories for their communication of the results of their studies of the quality of our crystals. The very valuable analytical work was performed by Gordon Townsend, of Airtron, Inc.

## Propagation of a Glow Discharge into the Annular Gap between the Discharge Tube Wall and the Cathode\*†

HARRY VERON† AND NATHAN WAINFAN

*Polytechnic Institute of Brooklyn, Brooklyn, New York*

(Received 16 September 1965)

Time-resolved spectroscopic measurements and electrostatic probe measurements were used to study that part of a high-voltage pulsed glow discharge in hydrogen that propagated into the annular gap between the cathode and the Pyrex discharge tube wall. The spectroscopic and probe measurements revealed that a luminous front and a potential wave started to propagate into the annular gap at the same time as the electric field in the cathode fall region at the face of the cathode reached its maximum value. The dependence of the propagation velocity on the discharge parameters is presented and the importance of the secondary emission at the wall of the discharge tube is established as a factor in the propagation of the discharge.

## INTRODUCTION

THE low-voltage glow discharge in gases has been most extensively studied by many investigators.<sup>1</sup> Among the more difficult measurements on these low-voltage "normal" glow discharges has been the measurement of the electric field distribution, particularly

within the cathode fall.<sup>2,3</sup> Recently, considerable attention has been paid to the highly abnormal glow in which the applied voltage far exceeds the normal starting potential. Within such abnormal glow discharges the electric fields within the cathode fall can reach many kilovolts per centimeter.<sup>4</sup> These large cathode-fall electric fields make possible field measurements via the Stark splitting of the spectral lines. For pulsed discharges in hydrogen such measurements can be made with sufficient time and space resolution so as to follow, in detail, the buildup of the pulsed discharge.<sup>5</sup> During the study of such high-voltage pulsed discharges in hydrogen, it

\* Taken in part from the dissertation submitted by one of the authors (H.V.) to the faculty of the Polytechnic Institute of Brooklyn in partial fulfillment of the requirements for the degree of Doctor of Philosophy, 1965.

† This work was supported in part by the U. S. Dept. of the Navy, Office of Naval Research under Grant AF-AFOSR-62-295, and the U. S. Air Force Cambridge Research Laboratories, Office of Aerospace Research under Contract No. AF-19(604)-7216.

‡ Present address: Cornell Aeronautical Laboratory, Inc., Buffalo, New York.

<sup>1</sup> M. J. Druyvesteyn and F. M. Penning, *Rev. Mod. Phys.* **12**, 87 (1940).

<sup>2</sup> R. P. Stein, *Phys. Rev.* **89**, 134 (1953).

<sup>3</sup> R. Warren, *Phys. Rev.* **98**, 1650 (1955).

<sup>4</sup> G. W. McClure, *Phys. Rev.* **124**, 969 (1962).

<sup>5</sup> M. Nahemow, N. Wainfan, and A. L. Ward, *Phys. Rev.* **137**, A56 (1965).

was found that the propagation of the discharge into the annular gap around the cylindrical cathode occurred at rates which could be orders of magnitude smaller than those rates associated with the breakdown in the interelectrode region. It is the purpose of this paper first to give the results of time-resolved spectroscopic measurements and electrostatic probe measurements made on that part of a pulsed glow discharge in hydrogen which propagated into the cylindrical annular gap between the cathode and the Pyrex discharge tube wall and second, to suggest some possible mechanisms involved in the initiation and evolution of the discharge in the annular gap.

Using the time-resolved spectroscopic measurements, the buildup of the luminosity of the discharge was determined as a function of position and time. The electric field at the face of the cathode and in the annular gap was measured as a function of position and time by measuring the Stark splitting of the hydrogen Balmer lines.

To yield further information about the nature of the discharge, measurements on the potential wave which accompanied breakdown in the annular gap were made using a series of external electrostatic probes. From the probe measurements the potential at the Pyrex wall of the discharge tube could be calculated for the discharge after breakdown. The data provided by the spectroscopic and electrostatic measurements were used to establish the importance of secondary mechanisms at the Pyrex walls in the development of the discharge in the annular gap around the cathode.

### EXPERIMENTAL TECHNIQUES

A diagram of the discharge tube and optical detection system is shown in Fig. 1. The system, as shown, is a modification of an apparatus used in previous studies in which the details of making time-resolved spectroscopic measurements are discussed.<sup>6</sup> Hydrogen pressure in the discharge tube could be varied from 0.2 to 3.0 Torr. The available annular gap between the aluminum cathode and Pyrex tube wall varied from 0.7 to 12.5 mm.

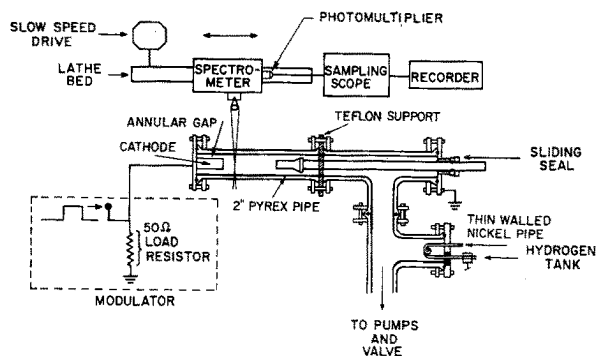
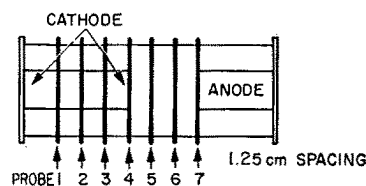
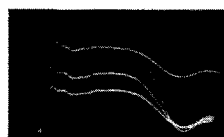


FIG. 1. Schematic diagram of the discharge tube and optical system.

<sup>6</sup> M. Nahemow and N. Wainfan, J. Appl. Phys. 34, 2988 (1963).



NO BREAKDOWN  
TUBE EVACUATED  $\sim 10^{-6}$  Torr  
SWEEP  $0.2 \mu \text{ sec/cm}$



APPLIED VOLTAGE 1000 volts/cm

PROBE 5 }  
PROBE 6 } 10 volts/cm

BREAKDOWN  
TUBE PRESSURE 0.86 Torr  
SWEEP  $0.2 \mu \text{ sec/cm}$



APPLIED VOLTAGE 1000 volts/cm

PROBE 1 }  
PROBE 2 } 20 volts/cm  
PROBE 3 }  
PROBE 4 }

FIG. 2. Ring probe system and the induced probe signals before and after breakdown.

A modulator supplied the discharge with pulses of 1.3- $\mu \text{sec}$  duration and a 60-nsec risetime. The pulse voltage could be varied from 500 to 5000 V. For this experiment the pulse repetition rate was maintained at 150 pulses/sec.

A Tektronix type 661 pulse-sampling oscilloscope was used to analyze the photomultiplier output from the spectrometer. The response time of the system was limited by that of the photomultiplier circuit which had an effective response time of 6 nsec and a delay of 37 nsec. The sampling intervals were 0.33 nsec wide and could be selected with an accuracy of approximately 1 nsec relative to the start of the applied voltage pulse.

With the arrangement shown in Fig. 1 the light intensity (as a function of wavelength) was measured for any selected time interval after the start of the applied voltage pulse and at any selected position in the discharge tube. The shape of the  $H_\beta$  line of the hydrogen spectrum thus obtained could yield the Stark splitting, and this in turn could yield the electric field.

With the slits of the spectrometer opened to accept all the radiation in a given spectral line, profiles of the integrated intensity of a particular spectral line were obtained as a function of axial position in the discharge tube for any selected time interval after the start of the applied voltage pulse. From these data the buildup of the luminosity in the discharge could be followed.

In order to further monitor the electrical breakdown in both the interelectrode region and the annular gap

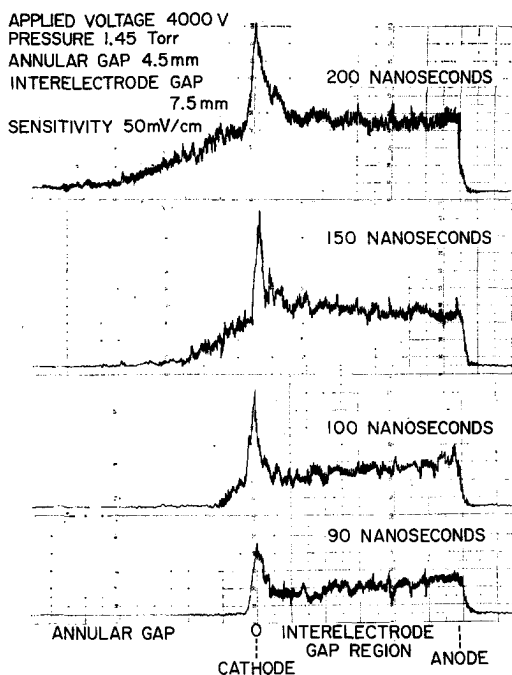


FIG. 3. Intensity of the unresolved  $H_\beta$  line as a function of position with the sampling interval as a parameter, from 90 to 200 nsec after the start of the voltage pulse.

and to determine the potential at the inner surface of the Pyrex discharge tube wall, a system of external electrostatic probes was devised.<sup>7</sup> This was done by placing a series of copper wire rings around the outside of the Pyrex discharge tube. A sketch of the probe arrangement is shown in Fig. 2. Any signal electrostatically induced on the ring probe was fed into a Tektronix type 551 oscilloscope through a coaxial cable. When electrical breakdown occurred, a change in the induced signal on the external ring probe was detected. The appearance of a step in the induced probe signal, as electrical breakdown occurred, was correlated with the measured propagation of the luminous front. The risetime of this oscilloscope and its associated electronics was approximately 14 nsec.

#### RESULTS OF TIME-RESOLVED SPECTROSCOPIC MEASUREMENTS (I)

By opening the exit slit of the spectrometer very wide, the integrated intensity of the  $H_\beta$  line as a function of time and axial position was obtained. Figure 3 shows these profiles of the light intensity as a function of axial position for a series of sampling intervals starting at 90 nsec after the beginning of the voltage pulse.

Earlier in time, approximately 50 nsec after the start of the applied voltage pulse, some electrical breakdown of the gas occurred approximately simultaneously in both annular and interelectrode gaps. At these early times the intensity of the  $H_\beta$  radiation from the inter-

electrode region was more than an order of magnitude larger than that from the annular gap. The initial breakdown of the gas in the interelectrode region was the same as that reported by Nahemow *et al.* for a discharge with no available annular gap around the cathode.

From the spatial profiles, such as shown in Fig. 3, the propagation velocity of the luminous front that traveled into the annular gap was determined. Figure 4 presents the propagation velocity of the luminous front as a function of pressure with the annular gap size as a parameter. From the data in Fig. 4 the propagation velocity is observed to increase with increasing pressure at constant annular gap, and to increase with increasing gap at constant pressure. The propagation velocity was also found to increase with increasing applied voltage at constant pressure. It was found that by reducing the gas pressure sufficiently the discharge was only sustained in the interelectrode region while no appreciable discharge occurred in the annular gap. For an applied potential of 3600 V, and an annular gap of 3.3 mm, the value of the gas pressure for such a cut-off was 0.2 Torr, and is indicated by the point labeled cut-off in Fig. 4.

#### RESULTS OF TIME-RESOLVED SPECTROSCOPIC MEASUREMENTS (II)

With the spectroscope slits set to yield the maximum usable resolution, time-resolved spectroscopic measurements were made on the radiation which came from the region just forward of the cathode face, and also from

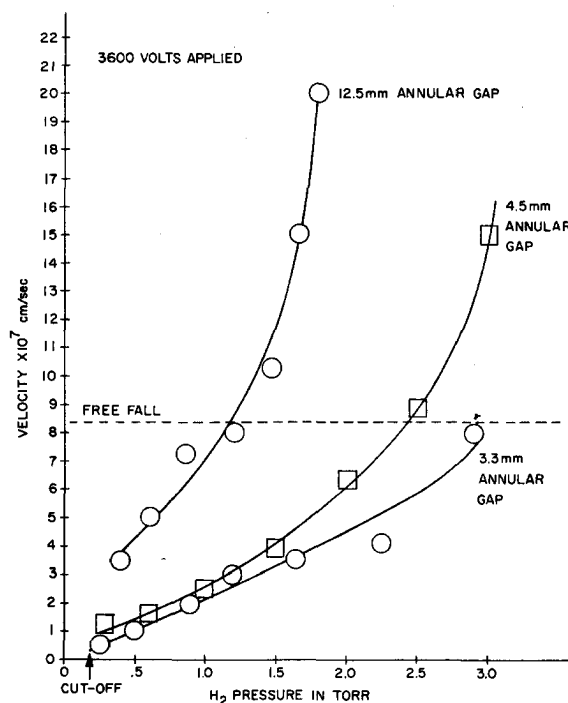


FIG. 4. Propagation velocity as a function of pressure with the annular gap as a parameter.

<sup>7</sup> A. Haberstick, Bull. Am. Phys. Soc. 9, 585 (1964).

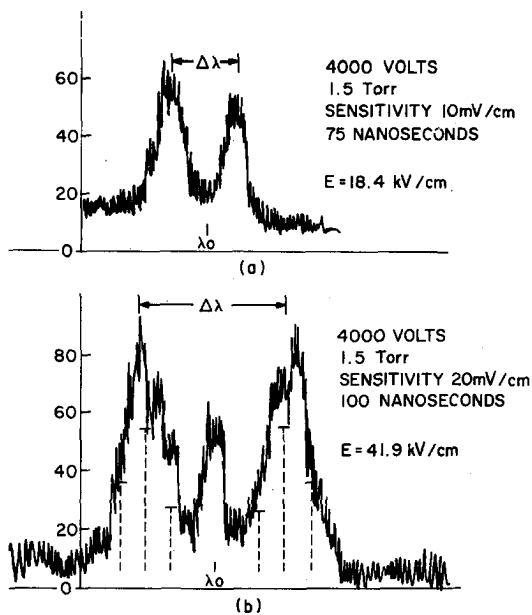


FIG. 5. Typical time-resolved  $\pi$  components of the Stark-split  $H_\beta$  line of the hydrogen spectrum at the cathode face: interelectrode gap 7.5 cm; annular gap 4.5 mm;  $\lambda_0 = 4861.3 \text{ \AA}$ .

the annular gap between the cathode and Pyrex tube walls. The light intensity was recorded as function of wavelength with the time after the start of the applied voltage pulse and the spectrometer position as parameters. As early as 75 nsec after the start of the applied pulse, the  $H_\beta$  radiation from the region near the face of the cathode showed an incompletely resolved Stark splitting which indicated the presence of a large electric field [see Fig. 5(a)]. For this study we used the components of the Stark-split  $H_\beta$  spectral line that were linearly polarized in the direction of the applied field, the  $\pi$  components. By measuring the separation between the peaks of the incompletely resolved Stark-split  $H_\beta$  line, as shown in Fig. 5, the electric field was obtained.

For a 7.5-cm interelectrode gap, a gas pressure of 1.5 Torr, and an applied voltage of 4800 V, the electric field at the face reached its maximum value (41.9 kV/cm) in approximately 100 nsec after the start of the applied potential. The values of the electric field and of the dimensions associated with the cathode-fall region corresponded to the values obtained by Nahemow and Wainfan for a discharge which occurred in the wall-bounded case with no available annular gap around the cathode.

In Fig. 5(b) we see that at about 100 nsec after the start of the applied voltage pulse an unsplit  $H_\beta$  spectral component appeared in the spectral profiles taken at the face of the cathode. The intensity of the unsplit part of the  $H_\beta$  line increased with time and, toward the end of the 1.3- $\mu$ sec applied voltage pulse, obscured the Stark-split  $H_\beta$  components.

As the luminous front propagated into the annular gap the current density at the cylindrical annular region

that surrounded the outer perimeter of the cathode face increased with time, whereas the current density at the cathode face remained constant with time. The excitation that was produced by the electron current issuing from the annular gap in this region also increased with time. By adjusting the position of the spectrometer to observe the radiation coming from the region near the cathode face and from the surrounding annular gap, it was determined that the unsplit  $H_\beta$  component did originate from the large electron current density issuing from the annular region that surrounded the outer perimeter of the cathode face.

The time-resolved spectroscopic measurements were extended into the gap region with the aid of an optical system which rotated and focused an image of the annular gap onto the entrance slit of the spectrometer. For example, for an applied potential of 4800 V and a tube pressure of 0.8 Torr, the electric field at the surface of the side of the cathode near the face, in a 4.5-mm annular gap, reached a maximum value of 31 kV/cm. With this arrangement, however, the spatial resolution of the spectrometer was poor because of the axial striations in the Pyrex tube.

As the spectrometer was displaced parallel to the axis of the discharge tube, away from the cathode face, back into the annular gap, a delay in the appearance of the electric field was observed. Within the limits of the resolution of the apparatus, the large electric field at the surface of the cylindrical side of the cathode appeared to accompany the luminous front that propagated into the annular gap.

## RESULTS OF THE ELECTROSTATIC PROBE MEASUREMENTS

The external electrostatic ring probes, shown in Fig 2, are essentially one part of a capacitive voltage divider. If no electrical breakdown occurs the voltage at the oscilloscope  $V_0$  is related to the modulator output voltage  $V_m$  by the relation

$$V_0 = [C_1 / (C_1 + C_2)] V_m. \quad (1)$$

In Eq. (1),  $C_1$ , which is a function of the position of the ring probe along the discharge tube axis, is the capacitance between the ring probe and the cathode;  $C_2$  is the combined capacitance of the oscilloscope and coaxial cable and has a value of 100 pF.  $V_m$  and  $V_0$  are negative with respect to the anode potential.

Under the conditions for which no electrical breakdown occurred, Fig. 2 shows that the induced signals on the ring probes matched the shape of the modulator output pulse. The upper curve in Fig. 6 shows the magnitude of the induced signal on the probe as a function of axial position for an evacuated tube (no breakdown). From the level portion of this curve the magnitude of the induced signal was observed to remain nearly constant with axial position in the annular gap region. From Eq. (1), therefore, the capacitance between the cathode

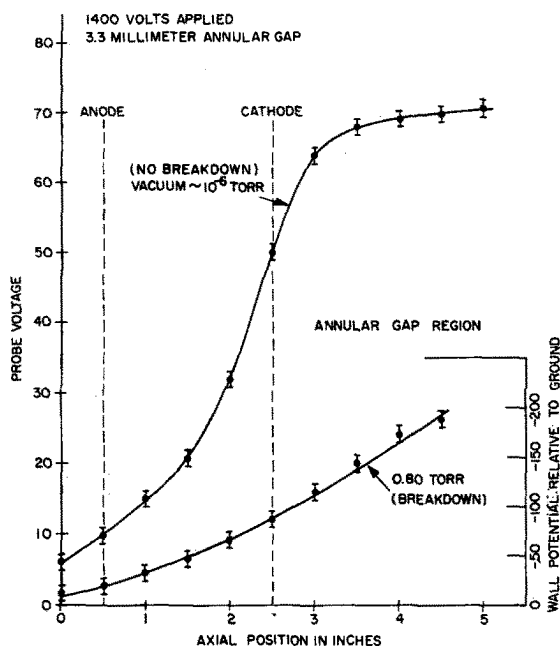


FIG. 6. Probe voltage as a function of axial position (before and after breakdown).

and ring probe was also nearly constant in the annular gap region. In this region  $C_1$  is equal to 4 pF. Also from Eq. (1) and the upper curve in Fig. 6, it is observed that as the anode was approached, the capacitance decreased as the distance between the probe and the cathode increased, particularly as the cathode face was crossed.

When hydrogen was diffused into the discharge tube and electrical breakdown occurred, a different situation resulted. The photographs in Fig. 2 show the change in the induced signal on the ring probes as the gas underwent electrical breakdown in the annular gap. By measuring the time interval between the potential steps that appeared on any two adjacent probes (see the sequential photographs in Fig. 2), the velocity of the potential wave accompanying electrical breakdown in the annular gap could be computed. The velocity of the potential wave was the same as the velocity of the luminous front that propagated into the annular gap. Moreover, the potential wave velocity showed the same dependence on pressure and applied voltage as the luminous front velocity showed in the annular gap region. The potential waves in the annular gap appeared to start at about 100 nsec after the start of the applied pulse which also corresponded to the behavior of the luminous front.

The potential wave that accompanied electrical breakdown in the interelectrode region propagated with a velocity greater than  $10^8$  cm/sec and could not be clearly resolved with the Tektronix 551 oscilloscope. These large propagation velocities in this region correspond to the known luminous front velocities in the interelectrode gap.<sup>5</sup>

In Fig. 2 we see that the step in the induced pulse appeared between two portions of the pulse that were each relatively constant with time. The magnitude of the level portion of the induced negative probe pulse after breakdown was smaller than that portion before breakdown.

After breakdown the external ring probes were electrostatically shielded from the cathode by the presence, in the discharge, of the ionized gas which had a large conductivity and small relaxation time. Evidence for this can be seen in the smooth transition of the lower curve in Fig. 6 as it crossed the position of the cathode face. In this state the external ring probe was capacitively coupled to the boundary region between the conducting gas and inner Pyrex tube wall. The capacitance for this configuration was 16 pF. Knowing this capacitance, the value of the wall potential  $V_w$  could be obtained.  $V_w$  was computed from the relation

$$V_w = [(C_1' + C_2)/C_1']V_0', \quad (2)$$

where  $V_0'$ , read directly from the oscilloscope, is the magnitude of the induced negative signal on the ring probe after breakdown,  $C_2$  is the same as that which appeared in Eq. (1), and  $C_1'$  is the capacitance between the ring probe and inner surface of the Pyrex tube wall.

The lower curve in Fig. 6 presents the wall potential as a function of axial position. The ordinate on the right side of the graph is the value of the wall potential and is negative with respect to the anode.

## DISCUSSION

From the data presented above we can now outline the gross features of the electrical breakdown of the hydrogen in the cylindrical discharge tube with an annular gap about the cathode. For the purposes of this discussion we take as a typical set of parameters an annular gap of 4 mm and an interelectrode spacing of 7.5 cm, a hydrogen pressure of 1 Torr, and an applied pulse voltage of 4000 V.

During the first 50 nsec a weak breakdown occurs throughout the gas. The observed light intensity at this time is about a factor of ten stronger in the interelectrode region than in the annular gap.

In the next 50 nsec there is a rapid buildup of ionization in the interelectrode region resulting in a collapse of the electric field into a thin cathode-fall region near the face of the cathode. By the time 100 nsec have passed, this collapse of the electric field is nearly complete. The electric field at the face of the cathode is then of the order of 30 kV/cm. This process in the interelectrode region appears to be identical to that reported previously for wall-bounded discharges with no available annular gap.

Starting at about 100 nsec an intense breakdown starts to propagate into the annular gap with a velocity of the order of  $10^7$  cm/sec. In company with the observed propagating luminous front we find a potential

wave and a high-field cathode-fall region at the surface of the cathode. As the discharge disturbance travels into the annular gap there is a rise in the discharge tube current. The increasing current issuing from the mouth of the annular gap is made evident by the strong, low-field excitation of the discharge at the mouth of the annular gap.

The propagation of the intense discharge into the annular gap depends in the following way on the discharge parameters. The propagation velocity increased with increasing pressure, increased with increasing gap size, and increased with applied voltage. There exists a lower pressure limit, about 0.2 Torr for the sample conditions, below which the intense breakdown in the interelectrode region would fail to propagate into the annular gap.

When the propagation of the discharge into the annular gap was complete and the discharge was in a state of quasi-equilibrium, the electrostatic probes were shielded from the cathode by the ionized gas. An axial potential gradient existed along the Pyrex wall around the annular gap (see slope of the lower curves in Fig. 6) and the entire cathode was enveloped by a positive-space-charge sheath. This latter point is made evident by the high-field cathode fall as elucidated by spectroscopic measurements and by the electrostatic probe measurements.

With the general morphology of the discharge presented above, we can now examine some of the implications of the results given. It is instructive to look into some of the mechanisms that must occur in the annular gap as the discharge propagates into it. With passing of the luminous front a high-field cathode-fall region is left at the surface of the cathode. Both from the evidence of the electric field distribution in the cathode fall and from the wall potential measurements, we find that approximately 80% of the applied potential appears across the cathode-fall region close to the cathode surface. The existence of this cathode fall implies that almost all the electrons leaving the cathode surface, due to the positive ion bombardment, attain an energy of several kilovolts in their transit through the cathode-fall region. Electrons of this energy have a free path, at the operating pressure used, that is many times the annular gap size.<sup>8</sup> Therefore almost all the electrons that leave the side of the cathode strike the Pyrex glass walls with energies of the order of kilovolts. Those electrons participating in multiplication and excitation processes within the gas must therefore be secondary emission electrons from the glass walls. The equilibrium potential of the glass walls is determined by the secondary emission characteristics of the Pyrex and the electron population and its energy distribution in the gas around the cathode. A requirement for a stable potential at the glass walls is that the net secondary electron emission

coefficient be unity. The current of energetic electrons from the cathode has a secondary emission coefficient greater than one.<sup>9</sup> The slow electrons collected from the gas (produced by secondary emission from the glass and ionization of the gas) yield a secondary emission coefficient less than unity. At equilibrium the fast and slow electrons bombarding the glass and their secondary products leaving the glass must yield a net current of zero to the glass walls. It is clear from these results that the secondary electron emission characteristics of the walls play an important role in establishing the discharge in the narrow annular gap. We find that after the discharge has propagated into the annular gap an axial potential gradient exists along the glass walls around the annular gap. This means that the potential fall at the side of the cathode (in the annular gap) is greatest near the cathode face and smallest near the back of the gap. This axial distribution of potential, caused by the electronic charge distribution in the gap, provides the axial electric field component necessary to drive the large electron current out of the annular gap.

Because of the cylindrical symmetry of the system and the complex boundary conditions, we have not been able to make a detailed calculation on the propagation of the discharge into the annular gap. We can, however, indulge in some speculation based on previous work and on the results presented in Fig. 4. For high pressures, or large annular gaps, the velocity of propagation of the discharge in the annular gap approaches values observed for breakdown in the interelectrode region. This breakdown in the interelectrode region has been successfully handled using a one-dimensional Townsend avalanche model, where continuous account was made of the formation of the electric field distribution.<sup>10</sup> It is, therefore, reasonable to believe that for large annular gaps the propagation velocity of the breakdown in the gap can be explained in terms of the same Townsend mechanisms used in the interelectrode region and the new boundary conditions. For small annular gaps or low pressures the velocity of propagation into the gap can be as small as  $3 \times 10^6$  cm/sec. These low velocities are suggestive of ion velocities after free fall through a potential difference of the order of a kilovolt. This observation in turn leads to the suggestion that under the low velocity conditions the rate at which the discharge propagates into the annular gap might be determined by an ion injection mechanism in which positive ions are injected into the annular gap by the fringing field at the edge of the already formed cathode sheath. The cathode sheath may then follow on the heels of the injected ions via the secondary emission processes at the cathode, and at the glass walls, and subsequent gaseous ionization.

<sup>9</sup> C. W. Mueller, J. Appl. Phys. **16**, 453 (1945).

<sup>10</sup> A. L. Ward, *Proceedings of the Fifth International Conference on Ionization Phenomena in Gases, Munich, 1961* (North-Holland Publishing Company, Amsterdam, 1962), p. 1596.

<sup>8</sup> W. L. Fite and R. T. Brackmann, Phys. Rev. **112**, 1141, 1151 (1958).